Monte Carlo based microscopic description of electron transport in GaAs/Al0.45Ga0.55As quantum-cascade laser structure

P. Borowik, Jean-Luc Thobel, L. Adamowicz

Monte Carlo based microscopic description of electron transport in $GaAs/Al_{0.45}Ga_{0.55}As$ quantum-cascade laser structure

Cite as: J. Appl. Phys. **108**, 073106 (2010); https://doi.org/10.1063/1.3488909
Submitted: 21 May 2010 • Accepted: 13 August 2010 • Published Online: 06 October 2010

Piotr Borowik, Jean-Luc Thobel and Leszek Adamowicz

Monte Carlo based microscopic description of electron transport in GaAs/$Al_{0.45}Ga_{0.55}As$ quantum-cascade laser structure

Piotr Borowik,[1] Jean-Luc Thobel,[2] and Leszek Adamowicz[1,a)]
[1]*Faculty of Physics, Warsaw University of Technology, ul. Koszykowa 75, PL-00-662 Warszawa, Poland*
[2]*Institute d'Electronique de Microélectronique et de Nanotechnologie, UMR CNRS 8520, Université Lille 1, Avenue Poincaré, BP 69, 59652 Villeneuve d'Ascq Cedex, France*

(Received 21 May 2010; accepted 13 August 2010; published online 6 October 2010)

Results of multiparticle Monte Carlo simulations of midinfrared quantum cascade lasers structure initially fabricated by Page *et al.* are presented. The main aim of this paper is to discuss in details how electric current flows through the structure and which subbands are involved in this process. Monte Carlo method allows to predict the electron population inversion between the lasing levels and gives microscopic insight into processes leading to such behavior. Importance of a subband belonging to the laser injector region, with energy slightly below the upper lasing level, is demonstrated. The electron–electron Coulomb interactions influence the shapes of electron distribution functions; the values of average electron energies and effective subbands' temperatures are calculated. © *2010 American Institute of Physics*. [doi:10.1063/1.3488909]

I. INTRODUCTION

Reliable simulation methods which can deal with the complicated physical phenomena involved in the quantum cascade lasers (QCL) operation are highly desired. The top goal would be to use such tools to predict the behavior of new structures and optimize their performances by better design. Another goal is the description of existing structures for better understanding of their properties. One of the most powerful tools for investigating charge transport in semiconductor materials and devices is the ensemble Monte Carlo (MC) method.[1,2] This approach has proven its utility in explaining the operation of devices such as field effect transistors or QCLs. Some characteristics such as, for example, subbands population, the number of scattering events between subbands, and many others, can be evaluated numerically, however are difficult if not impossible to be measured directly. Adapting this type of modeling to QCLs requires some additional assumptions as compared to more classical devices, but proved to be successful. First of all, since we are interested in studying electrons flow in the direction perpendicular to hetero-junctions, one needs to face a quantum transport problem. Hopefully, it has been shown that a Boltzmann-like formalism, neglecting coherent carrier dynamics, is quite sufficient, at least to describe the stationary state.[3] With such an approach, the major problem arises from the huge number of possible scattering paths.

Another commonly used theoretical tool which is suitable to study the properties of QCL structures is the rate equation (RE) method.[4–7] Both MC and RE approaches are based on the same physical picture concerning electron states and interactions. RE algorithm is much easy to implement and requires less computation resources comparing to MC method. However, it needs an assumption on the shape of electron distribution function, and usually it is Fermi–Dirac distribution. In MC method, nonequilibrium electron distribution function is obtained as a result of simulation. As MC method requires less *a priori* assumptions, we found it more suitable for the presented studies. The complete MC algorithm was already described in details elsewhere.[8]

In this paper, we studied the structure proposed by Page *et al.*[9] This structure, which is able to operate at room temperatures in pulsed, as well as in continuous mode up to 150 K,[10] is a good testbed for our MC model since it has been studied by several groups, and experimental and theoretical results are, therefore, available for comparison.

We discuss the results of our simulations with the aim to elucidate in more details how electron current flows through the structure and what mechanisms are responsible for building the population inversion between the lasing levels. Although qualitative description of the paths of electron transitions during their flow through various types of QCLs can be found in some papers,[4,5,11] we find it interesting and useful to describe in more details the results of complete MC simulations of this often studied QCL structure.

Several authors reported the results of the theoretical studies of population inversion.[4,5,11] However, these results were obtained for other structures and cannot be directly compared with our simulations.

II. MODELED STRUCTURE

Electron subband energies and wave-functions, used during MC simulations, are obtained by solving Schrödinger equation. The doping of the considered structure is very low (electron sheet density equal to 3×10^{11} cm^{-2}), therefore, the band bending induced by space charge can be neglected. This approximation allows us to save computation time, as the subbands positions, wave-functions, and scattering probabilities were calculated only once at the beginning of simulations.

The Schrödinger equation is solved for the structure containing three segments and subsequently, in the next step,

a)Electronic mail: adamo@if.pw.edu.pl.

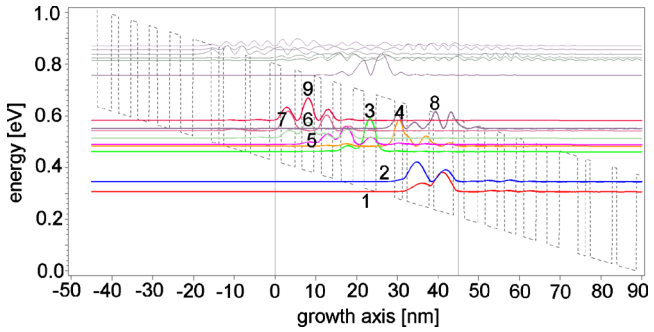

FIG. 1. (Color online) Calculated square moduli of wave-functions for central segment, shifted to show the position of respective energy level. The five lowest states are plotted in bold and labeled by numbers. *x*-axis represents distance along the growth direction, *y*-axis potential energy. The bottom of the conduction band, representing the studied structure potential, is drawn for three consecutive laser segments. The layers thickness sequence is as follows: 2.8/**3.4**/1.7/**3.0**/1.8/**2.8**/2.0/**3.0**/2.6/**3.0**/4.6/**1.9**/1.1/**5.4**/1.1/**4.8** (nm). The thicknesses for GaAs layers are highlighted by bold type. Other layers are fabricated of $Al_{0.45}Ga_{0.55}As$. Applied electric field is equal to 48 kV/cm.

each obtained wave-function is assigned to relevant segment according to its predominant localization within the segment. The subbands and wave-functions belonging to the middle segment are then shifted to neighboring segments; this procedure allows to impose periodic boundary conditions for the eigenfunctions. We used 15 energy levels per cascade segment, which in total gives 45 levels for the whole modeled system.

In Fig. 1, on the background picture of the potential shape, we present the calculated wave-functions shifted to the position of subbands bottom reference energies. The laser action in this structure occurs between the levels fourth and second, separated by 137 meV, and we concentrate on the population inversion between them. The first subband serves to collect electrons from lower lasing level and is separated from it by 40 meV. We can also notice that the collector second subband is separated from a group of upper injector and active region subbands, within the same segment, by remarkable energy difference 116 meV, which leads to an accumulation of electrons on the third subband as will be shown later. Furthermore, energy differences between consecutive subbands, in a group from third to ninth, are much smaller. Hence, on this account we expect to observe frequent electron transitions between these states due to various scattering mechanisms. We can also notice that tenth subband and upper ones are more similar to continuumlike states than to states bound in the quantum well, and are separated from lower subbands by quite high energy (175 meV).

III. MC MODEL

Our MC model accounts for acoustic and polar optical phonons as well as for alloy scattering mechanisms. During the simulation all electrons occupy the states belonging to the central segment but are allowed to be scattered to all subbands within this one and neighboring segments. When electron was scattered to a neighboring segment, it is moved to the corresponding subband in the central segment—the procedure which imposes the periodic conditions for the electric current.

Now, let us turn our attention to the algorithm used to account for carrier-carrier Coulomb scattering. Our model allows the scattering events to appear between two interacting electrons which occupy the subbands belonging to the central segment. However, the final subbands after scattering may belong to a neighboring segment. Calculation of the scattering probabilities with two-particle Coulomb interaction is difficult to implement in an algorithm in rigorous way. The probabilities depend on electrons distribution which is not known *a priori*, but is obtained in the course of simulations. The distribution function affects scattering rate in two different ways: it governs the distribution of partner electron, but it also has an indirect influence on the interaction potential through screening effect. The rigorous description of this effect would imply to invert the polarizability tensor, but this approach is very time consuming and may be numerically prohibitive for the systems with a large number of considered subbands. There are numerous approximate models for dielectric function which also allow including effects such as, for example, the screening by nonequilibrium electron gas or multisubband screening.[8,12,13] Nevertheless, in our model we decided to use a simple monosubband screening, accordingly assuming that the electron distribution function obeys Fermi–Dirac distribution[14,15] and that electron density on most occupied subbands is equal to total electron density in the structure. We also made some supplementary tests with an algorithm of self-consistent updating of electron effective temperature and quasi-Fermi level according to the electron distribution obtained during the simulation. After all it turned out that the difference in the results can be neglected; hence we have made the choice in favor of the simpler and faster algorithm. We will further discuss the reliability of the conditions assumed here.

Another important difficulty, that needs consideration, is the numerical problem caused by huge difference between phonons scattering rates and maximal electron–electron scattering rates. Let us notice that for lattice temperature of 150 K used in our studies, the probability calculated in the MC algorithm that an electron will be scattered to any other state in QCL structure, is of the order of 10^{13} s^{-1}, and the individual scattering rates due to a given scattering mechanism, for example polar optical phonons emission/absorption, are 1–2 orders of magnitude smaller. For the same conditions, the maximal electron–electron scattering rates are 3 orders of magnitude higher than total probability of phonon scattering. Even if such high maximal electron–electron scattering rate is used in the algorithm it does not mean that we have so many electron–electron scattering events, as most of them are rejected. In order to avoid artificial omission of the rare events, one must check that the precision of the random number generator is sufficient. Alternative methods based on rejection technique can also be used as last resort.

IV. SIMULATION RESULTS

One of important aims of the modeling of QCL is the prediction of subband population. As it is presented in Fig. 2,

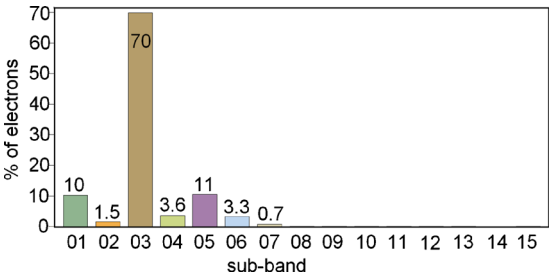

FIG. 2. (Color online) Calculated subband populations as percent of total carrier sheet density.

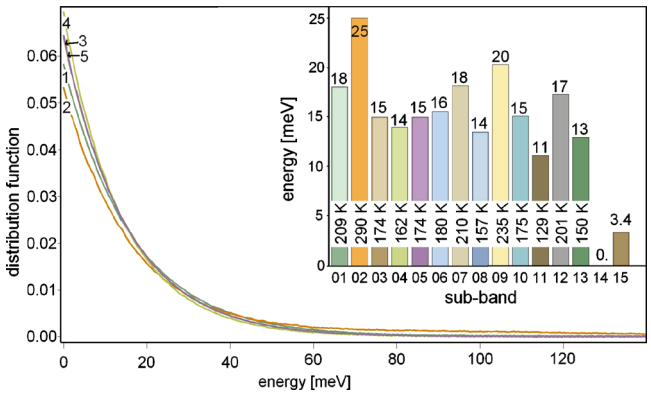

FIG. 3. (Color online) Shapes of electron distribution function for first five subbands. Populations on upper subbands are much lower and are not shown. The insert shows the average electron energies. Labels indicate energies in meV and corresponding effective temperatures in K.

our simulation predicts population inversion between the lasing levels fourth and second, as needed for laser radiation. We should admit that the calculated population inversion $N_{up}/N_{down}=2.4$ is different than the results reported by Schrottke *et al.*[16] Presented in their work calculations with rate-equation model give for structures with aluminum concentration $x=0.33$ and $x=0.45$ a value of 8 for this ratio. Their measurements for structure with $x=0.33$ give $N_{up}/N_{down}=2.6$, but indirect measurements for structure with $x=0.45$ lead to value $N_{up}/N_{down}=10$. Such difference between our MC model and RE calculations needs to be studied in more details. The measurements[16] were performed for transverse electric field equal to 60 kV/cm which was higher than the value reported in other references for the Page structure. Also their measured energy separation between lasing levels 144 meV differs from the value that we used in our calculations.

An interesting feature, observed in Fig. 2, is the accumulation of electrons on the third subband which is in fact the lowest injector level. This can be explained by the fact that when electrons arrive to this subband, and are thermalized by optical phonons emission and intercarrier scatterings, they have very low probability to be scattered to any lower subband. The closest underneath subband is one of the continuumlike states from the right neighboring segment and is separated by about 95 meV. However, overlaps of the wavefunctions for this state, as well as overlaps between subbands third and second wave-functions are very small, which results in a small electron transition probability. As we will demonstrate later the electron accumulation on this subband plays crucial role in building the population inversion between the lasing levels. The accumulation of carriers on this subband (88% for 77 K) was also reported by other authors as results of their RE studies.[6]

One notices that only seven or even six subbands are significantly populated. This result agrees with other studies[6,17] confirming that leakage from bound to Γ-valley continuum states is minimized. One might then be tempted to simplify the model by considering a reduced number of levels. However, as we will see later, before to conclude on this question a careful examination of scattering transfers is required.

Another issue that we would like to discuss is related to the average electron energies and distribution function shapes, which are presented in Fig. 3. Electron distribution functions for most populated subbands are very similar in shape to Fermi–Dirac function, or more specifically—taking into account quite high temperature and low electron density—to Boltzmann function. Also average kinetic energies for electrons in these subbands are very close to each other. This can be explained by the fact that electrons after being scattered to these subbands, stay there for sufficiently long time to reach the quasiequilibrium distribution. Of course, the average energy is higher than that corresponding to thermal equilibrium with the crystal lattice as there is a constant flow of highly energetic electrons from upper segments. The fact that average electron energies (or effective temperatures) are very close to each other, may also be an additional argument supporting the approximation of monosubband screening model for electron–electron scattering which was used in our calculations. The effect that electron temperatures on different QCL subbands are very close to each other was also reported by other studies both theoretical[14,15] and experimental.[18] Experimental studies[19] for the structure of Page reported electron temperatures of about 800 K at threshold when structure was measured with heat-sink temperature of 243 K and estimated lattice temperature was equal to about 300 K. As it was discussed by other authors,[20] it is not trivial to compare such results with theoretical models in the framework of used approximations. Another study[7] of electron temperature performed for room temperature conditions demonstrates similar order of values.

The equilibriumlike shape of the distribution function can explain another interesting feature that can be noticed. The results of simulations are practically the same regardless the electron gas temperature that was taken to calculate the dielectric constant used in electron–electron screening. Almost the same results were obtained after calculations with electron gas temperature equal to the lattice temperature (150 K) and with electron gas temperature obtained self-consistently in the course of the simulation (~180 K as it can be read from Fig. 3). First of all, the electron–electron scattering events are much more frequent than other interactions. They are elastic in nature so cannot change total electron gas energy but energy is exchanged between interacting carriers. In fact, the electron distribution within a given subband is mainly governed by electron–electron interactions.[15,21] When this scattering mechanism is frequent

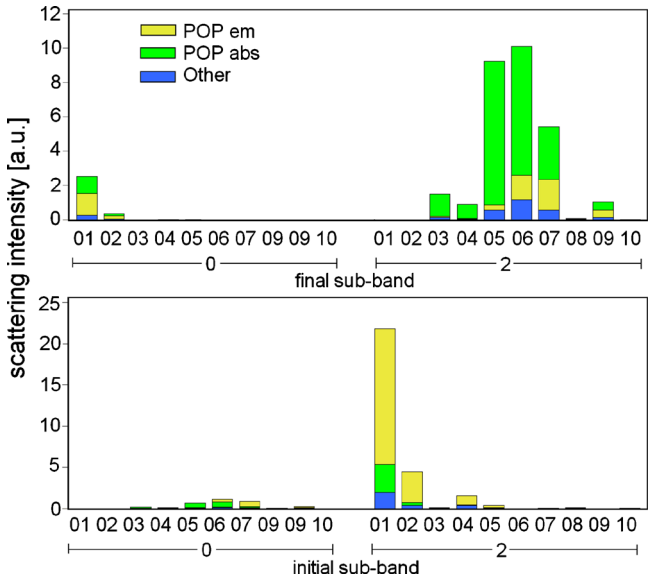

FIG. 4. (Color online) Relative frequency of scattering events for which the starting subband belongs to one structure segment and the target one belongs to a neighboring segment. Such events represent the electric current flowing throughout the laser structure. Upper chart shows what the final subbands of such intersegment events are. The left group denoted by 0 represents scatterings to the left neighboring segment which is equivalent to backward current. The right group denoted by 2 represents scatterings to the right neighboring segment which is equivalent to forward current. Lower chart displays the initial subbands of such scatterings to neighboring segment. The left group denoted by 0 represents the backward current. The right group denoted by 2 represents the forward current. Labels "POP abs," "POP em," and "other" mark, respectively, the contribution of scattering by absorption of polar optical phonons, emission of polar optical phonons, and joint scatterings by acoustic phonons and alloy potential.

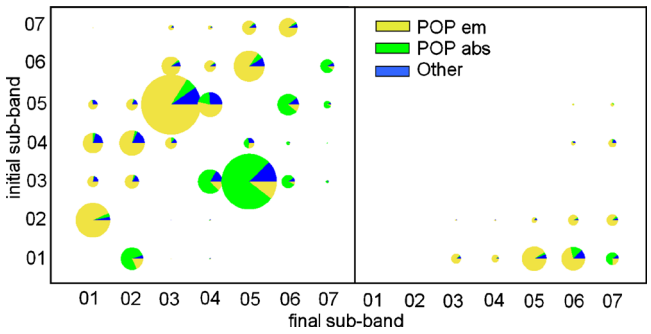

FIG. 5. (Color online) Intensity of scattering events between subbands. The size (area) of a given bubble represents the number of events. For each initial subband (*y*-axis) assign the final state after interaction—final subband (*x*-axis). The left part of the figure represents intrasegment scatterings; the right part, the scatterings to the right neighboring segment. Only scattering between first seven subband are plotted as scatterings to higher subbands are not visible in the scale of this figure.

enough, the distribution function tends to assume a "Fermi–Dirac" shape and is not significantly altered even when the electron–electron scattering rate further increases as a result of a less efficient screening.

Another interesting output of MC modeling is the detailed description of the current flowing between the neighboring segments. In the framework of this model, the current is represented by scattering events for which initial subband belongs to one segment and final subband after scattering belongs to a neighboring one. In Fig. 4, we present two charts demonstrating the current from two perspectives. From the first one, we can see what the final subbands of such transitions are. It is interesting to notice that above discussed results of subbands population are not sufficient to determine which subbands should be included in the simulation model. Certainly, the seventh subband, on which the electron population seems to be negligible, has a significant participation in the current. Even the current through the ninth subband is remarkable and this state should be considered in the model. Interestingly enough, a small backward current to first and second subband is observed in our simulations. The second perspective, in which intersegment current can be presented, shows what are the subbands from which these scatterings originate. First of all, we can observe that forward current originates mainly from the first subband and with much smaller intensity from the second one, which confirms that electrons in the first place relax within one segment to the lowest subband and only after that are scattered to a neighboring segment. There is also a small undesirable forward current flowing directly from the upper lasing level (fourth).

It is also interesting to verify how electrons behave during their flow through one cascade segment. In Fig. 5, we show the intensity of intersubbands scattering events. The intrasubband scatterings are omitted, as they only lead to electrons energy relaxation and do not directly influence the electron flow. First interesting finding is that we do not observed electron–electron scatterings which lead to the change in the subbands of interacting particles. Such processes were allowed but their probability is much smaller than probability of scatterings without changing subbands as well as smaller than intersubband scatterings due to interactions with polar optical phonons. One can also notice that elastic scattering mechanisms—acoustic phonons and alloy scattering—which were included in our model, have remarkable influence on the transport parameters and should not be neglected. In Fig. 5, we can notice, that in the region where polar optical phonon emission is a dominant scattering process (as for example, fifth to third subband transition), the number of elastic scattering events is similar, or even greater, than the number of polar optical phonons absorptions. As well in the region where polar optical phonon absorption is a dominant scattering process the number of elastic scattering events is comparable to the number of polar optical phonon emissions.

One of the aims of the QCL structure design is to optimize inversion population between lasing levels so that the maximum portion of the current should be directed to the fourth subband. Our above analysis of the intersegment current demonstrates that electrons arrive to subbands third–ninth. Let us first try to see what happens with electrons arriving to states above the upper lasing level. When we look at rows of bubbles in Fig. 5, representing scatterings from subband fifth and above, we can observe that these electrons fall down to the fourth subband which a desired effect is. There are also frequent scattering events with final state in the third subband. However, these electrons which are scattered to third subband are not lost and will still participate in building upper lasing level population. When we examine

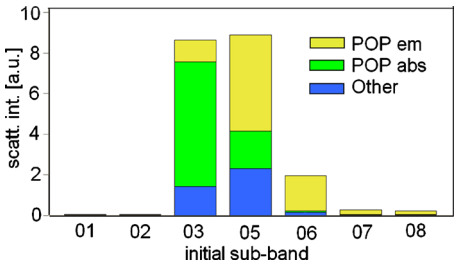

FIG. 6. (Color online) Scatterings responsible for filling upper lasing level. Scatterings starting from subbands higher than eighth, or from subbands belonging to neighboring segments are not visible in the scale of this figure.

the row of bubbles representing scatterings from third subband, we can notice that only a small portion of electrons falls down to first and second subband. Most of them are scattered back to upper subbands fourth–sixth and by this process they can terminate in the upper lasing level. Additional information that we can obtain from this figure concerns electrons which are transferred to lower subbands first and second. Columns of bubbles representing these events indicate that most of these charge carriers flow through the fourth subband. Our model did not include radiative emission process so we cannot judge how this process competes with nonradiative emptying of upper lasing level.

The proportion of current flowing through fourth subband to collector subbands to total current flowing through the structure can be a measure of effectiveness of injection to upper lasing level. From our calculations, we estimate this value to 61%. Other studies[22] present this value as a function of energy separation between upper lasing level and lowest injector subband and it varies from 60% to 95%.

Although, the following discussion can be deduced from previous figure our intention is to show in Fig. 6 only the scatterings which terminate in upper lasing level. There is a significant amount of electrons jumping from third level by absorption of polar optical phonon. But similar numbers of electrons arrive there from upper subbands fifth and sixth after emission of polar optical phonon. As energy of upper lasing level lies between energies of injector levels and their separation is quite small, we can also notice important flow of electrons via elastic scattering mechanisms—acoustic phonons and alloy scatterings.

V. CONCLUSIONS

Presented MC studies of QCL structure are able to predict the electron population inversion between the lasing levels. Our calculations demonstrated that in order to avoid an additional numeric bias on the results the simulation model should include about nine electronic subbands per a laser segment.

Our model allows us to describe in details what are microscopic effects responsible for electron current within the structure, what subbands and what scattering mechanisms are involved. We demonstrated the importance of the third subband with energy below the upper lasing level in creation of population inversion. The direct scatterings from this subband to the lower structure levels have very small probability. When electrons are collected on this subband they only rarely are directly scattered to the collector subbands and more often can be reinjected to upper lasing level thus increasing its population value.

It is interesting to observe the electron distribution functions on subbands and see the influence of electron–electron Coulomb scattering. This scattering is very important in the process of creation of the electron population inversion, but its influence is not direct. The observed number of intersubband electron–electron scatterings, leading to change in subband population is negligible. However, it has a crucial role in intrasubband electrons' relaxation to Boltzmann-like distribution and to equalization of electron energies between different subbands. In this way, the scatterings caused by other mechanisms are more frequent and the electrons' flow to the upper laser segment increases.

Extensions of this model are planned in order to give further insight in QCL operation. Probably the most interesting one would be the inclusion of laser action conditions and photon emission.[23,24] Our present studies can be interpreted as description of electric current conditions in the structure without optical resonator; extended model would describe an operating laser device. Also additional work is needed to compare in more details the differences between the results of MC and RE method.

ACKNOWLEDGMENTS

PB and LA acknowledge financial support from the Polish National Centre for Research and Development (Grant No. PBZ-MNiSW-02/I/2007).

[1] C. Jacoboni and L. Reggiani, Rev. Mod. Phys. **55**, 645 (1983).
[2] C. Jacoboni and P. Lugli, *The Monte Carlo Method for Semiconductor Device Simulations* (Springer, Wien, 1989).
[3] R. C. Iotti and F. Rossi, Phys. Rev. Lett. **87**, 146603 (2001).
[4] D. Indjin, P. Harrison, R. W. Kelsall, and Z. Ikonic, J. Appl. Phys. **91**, 9019 (2002).
[5] K. Donovan, P. Harrison, and R. W. Kelsall, J. Appl. Phys. **89**, 3084 (2001).
[6] D. Indjin, P. Harrison, R. W. Kelsall, and Z. Ikonic, Appl. Phys. Lett. **81**, 400 (2002).
[7] P. Harrison, D. Indjin, and R. W. Kelsall, J. Appl. Phys. **92**, 6921 (2002).
[8] O. Bonno, J. L. Thobel, and F. Dessenne, J. Appl. Phys. **97**, 043702 (2005).
[9] H. Page, C. Becker, A. Robertson, G. Glastre, V. Ortiz, and C. Sirtori, Appl. Phys. Lett. **78**, 3529 (2001).
[10] H. Page, S. Dhillon, M. Calligaro, C. Becker, V. Ortiz, and C. Sirtori, IEEE J. Quantum Electron. **40**, 665 (2004).
[11] F. Eickemeyer, K. Reimann, M. Woerner, T. Elsaesser, S.-C. Lee, A. Wacker, S. Barbieri, C. Sirtori, and J. Nagle, Physica B **314**, 314 (2002).
[12] J. T. Lü and J. C. Cao, Appl. Phys. Lett. **89**, 211115 (2006).
[13] R. Nelander and A. Wacker, J. Appl. Phys. **106**, 063115 (2009).
[14] P. Harrison, Appl. Phys. Lett. **75**, 2800 (1999).
[15] R. C. Iotti and F. Rossi, Appl. Phys. Lett. **78**, 2902 (2001).
[16] L. Schrottke, S. L. Lu, R. Hey, M. Giehler, H. Kostial, and H. T. Grahn, J. Appl. Phys. **97**, 123104 (2005).
[17] C. Sirtori, H. Page, C. Becker, and V. Ortiz, IEEE J. Quantum Electron. **38**, 547 (2002).
[18] M. Troccoli, G. Scamarcio, V. Spagnolo, A. Trediccuci, C. Gmachl, F. Capasso, D. L. Sivco, A. Y. Cho, and M. Striccoli, Appl. Phys. Lett. **77**, 1088 (2000).
[19] V. Spagnolo, G. Scamarcio, H. Page, and C. Sirtori, Appl. Phys. Lett. **84**,

3690 (2004).
[20]X. Gao, M. D'Souza, D. Botez, I. Knezevic, and J. Apl, J. Appl. Phys. **102**, 113107 (2007).
[21]C. Jirauschek and P. Lugli, Phys. Status Solidi C **5**, 221 (2008).
[22]V. D. Jovanović, S. Höfling, D. Indjin, N. Vukmirović, Z. Ikonić, P. Harrison, J. P. Reithmaier, and A. Forchel, J. Appl. Phys. **99**, 103106 (2006).
[23]C. Jirauschek and P. Lugli, J. Appl. Phys. **105**, 123102 (2009).
[24]C. Jirauschek, Appl. Phys. Lett. **96**, 011103 (2010).